Mixed Convection Heat Transfer in a Vertical Saturated Concentric Annulus Packed with a Metallic Porous Media

Dr. Mohammed A. Nima
Lecturer
Mechanical Engineering Department
College of Engineering- Baghdad University
E-mail: dralsafi@uobaghdad.edu.iq

Sarmad A. Abdal Hussein
Asst. Lecturer
Mechanical Engineering Department
Engineering College - Baghdad University
E-mail: sarmadaziz402@gmail.com

Saud S.Hameed
Mechanical Engineering Department
Engineering College - Baghdad University
E-mail: saudswedan@yahoo.com

ABSTRACT

Mixed convection heat transfer in a vertical concentric annulus packed with a metallic porous media and heated at a constant heat flux is experimentally investigated with water as the working fluid. A series of experiments have been carried out with a Rayleigh number range from Ra=122418.92 to 372579.31 and Reynolds number that based on the particles diameter of Re_d=14.62, 19.48 and 24.36. Under steady state condition, the measured data were collected and analyzed. Results show that the wall surface temperatures are affected by the imposed heat flux variation and Reynolds number variation. The variation of the local heat transfer coefficient and the mean Nusselt number are presented and analyzed. An empirical correlation has been proposed for computing the Nusselt number for the geometry and boundary conditions under investigation.

Key words: mixed convection, concentric annulus, metallic porous media, constant heat flux.

انتقال الحرارة بالحمل المختلط في تجويف حلقي عمودي مشبع ذو أسطوانتين متمركزتين تم حشوه بوسط مسامي معدني

المدرس الدكتور محمد عبد الرؤوف نعمة
قسم الهندسة الميكانيكية
كلية الهندسة – جامعة بغداد

المدرس المساعد سرمد عزيز عبد الحسين
قسم الهندسة الميكانيكية
كلية الهندسة – جامعة بغداد

سعود سويدان حميد
قسم الهندسة الميكانيكية
كلية الهندسة – جامعة بغداد

الخلاصة

انتقال الحرارة بالحمل المختلط في تجويف حلقي عمودي ذو أسطوانتين متمركزتين تم حشوه بوسط مسامي معدني قد تم دراسته بصورة عملية مع استخدام الماء كمائع مشغل. تم اجراء عدد من التجارب العملية لمدى رقم رالي من 122418.92 الى 372579.31 و مدى رقم رينولد على اساس قطر الجسيمات 14.62, 19.48 و 24.36. عند وصول حالة الاستقرار تم جمع البيانات وتحليلها. اظهرت النتائج تأثر درجات حرارة السطح تتأثر بتغير الفيض الحراري المسلط وتغير رقم رينولد. تغير معامل انتقال الحرارة الموضعي ومتوسط رقم نسلت قد تم اظهارها و دراستها. تم اقتراح معادلة تجريبية لحساب رقم نسلت للشكل الذي تم دراسته مع الظروف الحدية المحيطه به.

الكلمات المفتاحية: الحمل المختلط، أسطوانتين متمركزتين، وسط مسامي معدني، فيظ حراري ثابت.

1. INTRODUCTION

Heat transfer in porous media received great interest for many years because of the improved in the heat transfer performance without proportionate increase in hydraulic resistance. It is well known that the porous structure reduces the thickness of the boundary layer, increases the surface area that in contact with the fluid and intensifies the mixing of the flowing fluid, and thus enhances the thermal heat transfer. Flow and heat transfer through channels packed with porous media are widely studied because of their potential applications in thermal management such as compact heat electronic exchanges, solar collector, nuclear reactor cooling and regenerators. Packed bed has been developed for different types of porous materials with specific intent to enhance the heat transfer from the thermally loaded surfaces. Because of the random structures of porous media, they will be different in engineering, physical and thermal properties, **Venugopal, et al., 2010**. As a result, flow and heat transfer characteristics in these media also greatly differ. **Renken and Poulikakos**, **1990** investigated experimentally and numerically the forced convection heat transfer in the packed bed areas of an occupied parallel plate channel whose walls maintain a constant temperature. Based on this study, porous media needs to be considered as a viable alternative for the transfer of heat enlarge in forced convection heat transfer in channels. **Pu, et al., 1999,** used R-113 loop in performing the experiments of mixed convection heat transfer in a vertical packed channel with asymmetric heating of opposing walls. Chrome steel beads of 6.35 mm in diameter were used as a porous media. The experiments were carried out in the range of $2<Pe<2200$ and $700<Ra<1500$. The measured temperature distribution indicated the existence of a secondary convective cell inside the vertical packed channel in the mixed convection regime. A correlation equation for Nusselt number in terms of Peclet number Pe and Rayleigh number Ra was obtained from experimental data. They found that the following three convection regimes exist: natural convection regime: $105< Ra/Pe$, mixed convection regime: $1<Ra/Pe<105$, and forced convection regime: $Ra/Pe< 1$. **Dirker, 2000** presented a comparison of the literature that involving heat transfer in the ring. Their comparison showed that there was a need for more research in the field of links convection heat transfer in concentric ring as they found a little agreement among the existing relationship. Empirical relationship for predicted Nusselt number in the ring had been developed with water as the working fluid. **Boomsma and Poulikakos, 2002** showed the results of experimental studies performance to assess the hydraulic characteristics of open cell aluminum foam of different pore diameters and pore in each of the compressed and non-compressed format. The study was done mainly to predict important parameters permeability coefficient foam, precisely in order to describe the pressure drop versus the flow behavior in the porous media. **Hussein, et al., 2009** experimentally and theoretically studied the convective heat transfer in vertical concentric annulus where the two cylinders filled with porous medium. They concluded that the behavior of temperature profile were the same for any diameters ratio and any different heat flux. The relation between Nu and Ra was proposed and the results showed good agreement between experimental and theoretical studies. The potential of a

simple and inexpensive porous insert was experimentally investigated by **Venugopal, et al., 2010**. The porous inserted consists of a stack of metallic perforated plates that used to enhance the heat transfer from the heated wall of a vertical rectangular duct under forced flow conditions. The characteristic features of the porous medium model on the hydrodynamic and heat transfer behavior were investigated. The key novelty in this work was the development of a new correlation for the Nusselt number that did not require any information from hydrodynamic studies. The largest increase in the average Nusselt number of 4.52 times that for clear flow was observed with a porous material of porosity of 0.85. **Andrea, et al., 2012,** investigated experimentally the air forced convection through electrically heated open-cells copper foams with different number of pores per unit of length (PPI) with constant porosity (ε=0.93) and foam core height of 40 mm. The experimental heat transfer coefficient and pressure drop measurements permitted to understand the effects of the pore density on the heat transfer and fluid flow performance of the foams. They compared different enhanced surfaces, which can be considered suitable for electronic thermal management against present author's experimental measurements for 40 mm high aluminum foams at the same operative test conditions.

To the best of the authors' knowledge, there is no existing experimental study on the mixed convection heat transfer in a saturated concentric annulus that filled with metallic porous media. So we proposed the present study to cover this shortage in the understanding of the flow and heat transfer in porous enclosure with mixed convection effects.

In the present work, mixed convection heat transfer in a vertical saturated concentric porous annulus subjected to a constant heat flux, is examined experimentally with water as the working fluid. The main objective is to study the influence of mixed convection heat transfer on the flow field and the associated heat transfer process in such system. The influence of heat flux and mass flux variation on wall temperatures and Nusselt number are investigated and analysed then a general relation that describe the overall process is presented.

2. EXPERIMENTAL APPARATUS AND PROCEDURE

2.1 Experimental Apparatus

The experimental investigation is carried out in an apparatus shown in **Figs. 1** and **3**. The apparatus has been constructed to achieve the requirements of the present study and it consists of the following major assemblies:

1- Test section

As shown in **Fig. 2**, the test section consists of two stainless steel cylinders that form a concentric annulus of length L=63 cm. The inside and outside diameters of inner cylinder are (D_i=40 mm, D_o=41mm) and the inside and outside diameters of outer cylinder are (D_i=80 mm, D_o=82 mm). The inner and the outer cylinders are assembling together by means of two Teflon flanges to form the concentric annulus test section. The Teflon flanges is used to reduce the dissipative heat transfer from the test section ends and to support the inner and outer cylinders in one concentric annulus by pushing them between the Teflon flanges inner and outer diameters (D_i=39 mm, D_o=83 mm). The wall thickness of each Teflon flange is 1.5 cm. Four holes are drilled in each

Teflon flange as shown in **Fig. 2** but with different purposes. The holes in the lower flange are used to distribute the incoming water from the liquid splitter and guide it uniformly to inter the test section, while the holes in the upper flange are used as an exit passage for the thermocouples extension wires that used to measure inner cylinder wall temperatures. The upper flange holes are filled with a relatively high temperature adhesive material to support the thermocouples extension wires and to prevent water infiltration. The concentric annulus is packed with stainless steel beads, essentially spherical in shape with an average particles diameters of d_p=6 mm. A metallic O-Ring with holes (less than 6mm in diameter) is used to support the metallic porous media 13.5 cm far from the test section lower end and to form an entrance length to achieve a uniform inlet water velocity profile to the porous packing. The length of the porous packing was designed to be 40 cm as shown in **Fig. 2**, and the water was then derived out of the test section by a tube that mounted at 9.5 cm far from the test section upper end. A uniform heat flux is provided on the outer surface of the concentric annulus by a nickel-chrome wire of 1 mm in diameter, which is electrically insulated and warps around the outer surface of the concentric annulus along the test section part that filled with the metallic porous media (40 cm). This steel wire is supplied with AC-current from a voltage regulator, to control the incoming current according to the heat flux desired. The test section is well insulated outside with asbestos and fiber glass wool layers of 15 mm and 50 mm thickness, respectively. The concentric annulus outer surface and inner surface temperatures are measured by (18 K-type) thermocouples, which were distributed equally within nine sections along the outer surface and inner surface of the concentric annulus as shown in **Fig. 2**. Another (5 K –type) thermocouples were used to measure the water bulk temperature distribution by inserting these thermocouples inside the test section through holes on the outer surface of the concentric annulus as shown in **Fig. 2**. These holes are filled with a relatively high temperature adhesive material to support the thermocouples extension wires and to prevent water infiltration. The temperature distribution on the outer surface of the insulation shield are measured using (4 K-type) thermocouples distributed in an equal pitch, to calculate the heat lost during the experiment by referring to the temperature difference between the heater wall and the ambient. The heat lost is found to be approximately 6% during the whole range of the imposed heat flux. A digital electronic thermometer (type IDC-420042), is connected in parallel to the thermocouples by leads through a selector switches, to record the temperature measurements.

2- Water supply

As shown in **Fig. 1**, the liquid supply assembly consists of water tank, valve, filter, flowmeter (0.8 LPM full range) and liquid splitter, which are placed adjacent to the test section. A drain reservoir was placed at the test section exit to collect the water. When the water exit from the test section, it was forced to flow through a flexible tube that raise the water to a higher elevation (ΔH) before it collected in the drain reservoir. The purpose of this arrangement at the test section exit is to control the test section pressure and to ensure that the water pressure inside the test section is higher than the atmospheric pressure.

3- Electrical power measurement

The constant heat flux is supplied by using electrical circuit of alternating current that includes:

A) Voltage regulator.
B) Transformer.
C) Voltmeter.
D) Ammeter.

2.2 Experimental Procedure

Before starting the experimental measurements and in order to degas the air from the packed annulus, the valve is opened in such a manner that the water flow at the flowmeter full range (0.8 LPM) and a moderate heat flux is applied for two to three hours. Then, the valve is adjusted to give the required water flow rate. Each experiment is performed using the following procedure:

1) The valve that connected to the water tank is adjusted to give the required water flow rate which is measured by the flowmeter.
2) The electrical power is switched on, and the heater input voltage is adjusted by a voltage regulator to give the required voltage and current.
3) The supplied voltage and current to the heater are recorded to calculate the required electrical power in accordance to the heat flux required.
4) The apparatus is left for two to three hours to establish the steady state condition. The thermocouples readings are collected every half an hour. When the difference between two readings became almost constant, the steady state condition is fixed and a final reading is recorded.

To obtain a new set of experiments under the same water flow rate, a new electrical power is selected, and the procedure from step 2 to 4 is repeated.

The net heat flux to the saturated porous media is determined from recording the electrical power supplied to the heater and applying the following equation:

$$q_w = P_o/A \quad (1)$$

where;

P_o= electrical power consumed by heater = $I \times V$.

I = current flow through the heater.

V = voltage across the heater.

A = surface area of the annulus outer cylinder.

Heat losses from the heater across asbestos and fiber glass wool layers are calculated to be 6% while the heat losses from the axial direction through the Teflon flanges are found to be small and neglected. These losses are subtracted from the electric power to obtain the net heat transfer rate.

3. HEAT TRANSFER CALCULATIONS

It is important to calculate the absolute permeability (K), the effective thermal conductivity (k_{eff}) and the porosity (ε) of the saturated porous media, as they are used in the dimensionless groups that govern the fluid flow and heat transfer calculations.

According to **Nield and Bejan, 2006**:

$$K = \frac{\varepsilon^3 d_p^2}{180(1-\varepsilon)^2} \quad (2)$$

$$k_{\text{eff}} = \varepsilon k_l + (1-\varepsilon)k_s \quad (3)$$

where k_l and k_s are the thermal conductivities of the water and the solid porous media, respectively. The porosity of the packed stainless steel beads is found experimentally using the expression, **Nield and Bejan, 2006:**

$$\varepsilon = \frac{Vol_{total} - Vol_{solid}}{Vol_{total}} \quad (4)$$

3.1 Reynolds Number

The Reynolds number can be defined according to the particle diameter and the fluid velocity at the inlet as:

$$Re_d = \frac{U_{in} d_p}{v} \quad (5)$$

3.2 Grashof and Rayleigh Number

The Grashof number can be defined as:

$$Gr = \frac{g\beta K q_w D_h^2}{k_{eff}\, v^2} \quad (6)$$

then Rayleigh number (*Ra*) can be calculated using the following equation:

$$Ra = Gr\ Pr \quad (7)$$

3.3 Local and mean Nusselt Number

The local heat transfer coefficient at the heated wall can be defined as:

$$h = \frac{q_w}{T_w - T_b} \quad (8)$$

Hence, the local and the mean Nusselt number can be calculated as, **Nield and Bejan, 2006** :

$$Nu = \frac{h\, D_h}{k_{eff}} = \frac{q_w\, D_h}{k_{eff}\,(T_w - T_b)} \quad (9)$$

$$Nu_m = \frac{1}{L}\int_0^L Nu\ dy \quad (10)$$

The thermophysical properties of the water-stainless steel beads that used in the present study are listed in **Table 1** and the physical parameters for the stainless steel beads are listed in **Table 2**.

4. RESULTS AND DISCUSSION

A series of experiments have been carried out with a heat flux range from q_w = 3912 W/m^2 to 11907 W/m^2 (Ra=122418.92 to 372579.31) and volumetric flow rate of Q = 0.3, 0.4 and 0.5 L/min (Re_d=14.62, 19.48 and 24.36). The temperature distribution along the inner and the outer annulus surfaces is measured and presented. The influence of heat flux variation and Reynolds number variation on the local and mean heat transfer coefficient is discussed and analyzed. Finally, a general correlation for the mean Nusselt number Nu_m as a function of the parameters (*Ra*/*Re*) is derived to describe the overall fluid flow and heat transfer behavior in the porous annulus.

4.1 The Influence of Heat Flux and Reynolds Number on the Surface Temperature Distribution.

Figs. 4-6 show the influence of the imposed heat flux variation on the distribution of the outer annulus surface temperature for Re_d=14.62, 19.48 and 24.36, respectively. A general trend can be seen from **Figs. 4-6**, that the outer annulus surface temperature increases as the heat flux is increased for the same Reynolds number value. When the imposed heat flux is increased (with a constant Reynolds number), the buoyancy effect increases and causes a faster growth in the thermal boundary layer along the porous annulus surface that will be associated with an increased in the outer annulus surface temperature values.

Figs. 7-9 show the influence of the imposed heat flux variation on the distribution of the temperature difference between the outer and the inner annulus surface temperature [$\Delta T_w = T_{w,\ outer\ annulus\ surface} - T_{w,\ inner\ annulus\ surface}$] for Re_d=14.62, 19.48 and 24.36, respectively. **Figs. 7-9** show that the temperature difference (ΔT_w) increases as the imposed heat flux is increased for the same Reynolds number. It is clear from **Fig. 7,** that for a low Reynolds number (Re_d=14.62) the fluctuation in the temperature difference (ΔT_w) values with the axial distance is mild except for q_w = 11907 W/m^2. When the heat flux is supplied on the outer annulus surface, the buoyance force will caused an induced mass flux that will oppose the incoming cold-fluid and drive the hot fluid from the vicinity of the outer heated wall towards the inner insulated wall and rising its temperature. For low Reynolds number values, the buoyance effect increases and results in a faster heat transfer from the outer to the inner annulus surface and as a consequence a smaller temperature difference (ΔT_w) as shown in **Fig. 7**.

While for a higher Reynolds numbers of Re_d=19.48 and 24.36 **Figs. 8** and **9**, the temperature difference (ΔT_w) increases with the axial distance and reaches its maximum value at Z=0.2 m from the annulus entrance section and then it decreases downstream up to the annulus exit section. This behavior can be explained based on the interaction between the buoyancy force and the inertia force of the incoming cold-fluid. In the annulus entrance region the buoyancy force is still limited in comparison with the inertia force of the incoming cold-fluid, and this will caused a retreat in the thermal boundary layer growth from the outer annulus surface towards the inner annulus surface. The domination of the incoming cold-fluid effect in the entrance region will cause a faster temperature rise in the outer annulus surface and continues increased in the temperature difference (ΔT_w) with the axial distance to a point located at Z=0.2 m from the annulus entrance section as shown in **Figs. 8** and **9**. In the region downstream of Z=0.2 m, the buoyancy force becomes stronger due to the continuous heating and it will be able to overcome the inertia force of the incoming cold-fluid. This will result in mobilizing more hot fluid from the vicinity of the outer heated wall towards the inner insulated wall to rise its temperature and consequently we observe a remarkable decreased in the temperature difference (ΔT_w) as shown in **Figs. 8** and **9**. Another observation is made from **Figs. 7-9**, that for higher Reynolds numbers (Re_d=19.48 and 24.36) the temperature difference (ΔT_w) increases suddenly at the annulus exit section. This can be attributed to the higher fluid mixing at the annulus exit section as the hot fluid try to find its way out through the drain tube and this caused a

reduction in the inner annulus surface temperature and an increased in the temperature difference (ΔT_w) at the annulus exit.

Figs. 10-14 show the influence of Reynolds number variation on the distribution of the outer annulus surface temperature for q_w = 3912 W/m^2 to 11907 W/m^2. The figures show that the surface temperature decreases as the Reynolds number increased for the same heat flux value. When the Reynolds number increased the thermal boundary layer retreat along the heated wall and as a consequence a higher heat transfer rate can be expected that associated with a decrease in the outer annulus surface temperature.

Figs. 15-19 show the influence of Reynolds number variation on the distribution of the temperature difference between the outer and inner annulus surface temperature [$\Delta T_w = T_{w,\ outer\ annulus\ surface} - T_{w,\ inner\ annulus\ surface}$] for q_w = 3912 W/m^2 to 11907 W/m^2. Two different relationships between the temperature difference curves (ΔT_w) can be seen depending on the magnitude of the imposed heat flux.

At low heat fluxes, q_w = 3912 W/m^2 and 5511 W/m^2 **,Figs. 15** and **16**, the temperature difference (ΔT_w) decreases as the Reynolds number is increased except at Z=0.2m. For low heat fluxes the buoyancy effect is limited and the thermal boundary layer will grow in the vicinity of the heated wall only, and as a result the inner annulus surface temperature will mainly effected by the incoming cold-fluid. As the Reynolds number increased, the heated wall (outer annulus surface) temperature will decreases due to the incoming cold-fluid effect and the temperature difference (ΔT_w) between the outer and inner annulus surface will decrease as shown in **Figs. 15** and **16**.

While for higher heat fluxes, q_w = 7382 W/m^2 to 11907 W/m^2 **,Figs. 17-19**, a gradual inversion can be seen in which the temperature difference (ΔT_w) decreases as the Reynolds number is decreased. For high heat fluxes the buoyancy force is dominant over the inertia force of the incoming cold-fluid throughout the porous annulus. As the Reynolds number is decreased, the buoyancy effect more increases and causes a rapid movement of the hot fluid from the vicinity of the outer heated wall towards the inner insulated wall rising its temperature and reducing the temperature difference (ΔT_w) as shown in **Figs. 17-19**.

Figs. 15-19 also show that the temperature difference (ΔT_w) values at the annulus exit section are always higher for Re_d= 24.36 and then decreases as the Reynolds numbers is decreased. As mentioned earlier, when the hot fluid try to find its way out from the annulus exit section through the drain tube, a reduction in the inner annulus surface temperature is recorded due to the reduction in the hot fluid amount that mobilized from the vicinity of the outer heated wall towards the inner wall. This reduction in the inner annulus surface temperature increases for higher Reynolds numbers and causes the temperature difference (ΔT_w) at the exit section to be maximum at Re_d= 24.36.

4.2 Local Heat Transfer Coefficient.

A general behavior can be seen from the distribution of the local heat transfer coefficient in **Figs. 20-25**, that the local heat transfer coefficient decreases from the channel inlet to a point where it reaches its minimum value and then it increases downstream up to the channel exit. At the channel inlet, the small thickness of the thermal boundary layer results in high temperature gradients at the

heated wall and high heat transfer coefficient. As the thickness of the thermal boundary layer increases downstream, the heated wall temperature gradients decreases and causes a reduction in the heat transfer. As a result, the local heat transfer coefficient reaches its minimum value, after which the porous media plays a crucial role in the enhancement of heat transfer by conducting more heat from the heated wall to increase the fluid bulk temperature and as a consequence increases the local heat transfer coefficient values up to the channel exit.

Figs. 20-22 show the influence of the imposed heat flux variation on the distribution of the local heat transfer coefficient at the heated wall for Re_d=14.62, 19.48 and 24.36. It can be seen from these figures that the local heat transfer coefficient increases as the heat flux is increased for the same Reynolds number value. This can be attributed to the fact that for higher heat fluxes the buoyancy effect increases and the thermal boundary layer growth is more rapidly and causes a smaller temperature difference between the fluid bulk temperature and the heated wall temperature and as a result a higher local heat transfer coefficient will be attended.

Figs. 23-25 show the influence of Reynolds number variation on the distribution of the local heat transfer coefficient at the heated wall for q_w = 3912 W/m^2, 7382 W/m^2 and 11907 W/m^2. It can be seen from these figures that the local heat transfer coefficient increases as the Reynolds number is increased for the same heat flux value. When the Reynolds number is increased, a reduction in the thermal boundary layer thickness occurs with the domination of the incoming cold-fluid effect and this will cause a larger fluid mixing and higher local heat transfer coefficient values.

Another observation is made from **Figs. 23-25**, that the point of the minimum value of local heat transfer coefficient is moving towards the channel inlet as the imposed heat flux is increased. At q_w = 3912 W/m^2 **,Fig. 23**, the the local heat transfer coefficient curves reaches its minimum value at Z=0.2 m from the annulus entrance section, while this point is moving to Z=0.1 m at q_w = 7382 W/m^2 **,Fig. 24** and Z=0.05 m at q_w = 11907 W/m^2 **,Fig. 25**. As the heat flux increases, the buoyancy force increases and its effect start to arise from the channel inlet and causes an increase in the local heat transfer coefficient values and as a consequence a retreat in the point of the minimum value of local heat transfer coefficient towards the channel inlet.

4.3 Mean Nusselt Number.

The relationship between mean Nusselt number and Rayleigh number are plotted in **Fig. 26** for Re_d=14.62, 19.48 and 24.36. It shows an increase in the mean Nusselt number as Rayleigh number is increased for the same Reynolds number value. This can be attributed to the increase of the buoyancy effect for higher Rayleigh number values which improves the heat transfer process.

The relationship between mean Nusselt number and Reynolds number are plotted in **Fig. 27** for Ra=122418.92 to 372579.31, which shows an increase in the mean Nusselt number as Reynolds number is increased for the same Rayleigh number value. This can be attributed to the higher fluid mixing that associated with the domination of the incoming cold-fluid effect, which causes a clear heat transfer enhancement for higher Reynolds number values.

4.4 Correlation of Average Heat Transfer Data.

The values of the mean Nusselt number (Nu_m) are plotted in **Fig. 28** against (Ra/ Re_d) for the range of Ra=122418.92 to 372579.31, and Re_d=14.62 to 24.36. All the points as can be seen are represented by linearization of the following equations:

$$Nu_m = c(Ra/Re_d)^m \quad [c = 2.227 \,\&\, m = 0.144] \tag{11}$$

It can be seen from **Fig. 28** that the correlated mean Nusselt number increases with the increasing of Rayleigh number and Reynolds number.

5. COMPARISON WITH PREVIOUS EXPERIMENTAL RESULTS

K. Muralidhar, 1988 conducted a theoretical study on the mixed convective heat transfer in saturated porous annulus, where the inner cylinder is heated and the outer cylinder is cooled. This work is the closest previous published work that found in the literature using the same setup with mixed convection except that it is a theoretical study and the fluid is heated at a constant temperature along the inner cylinder. The average Nusselt number of a vertical annulus as a function of Rayleigh number for different Peclet numbers is shown in **Fig. 29**. It can be seen from **Fig. 29** that the average Nusselt number increases when the Rayleigh number is increased and when the Peclet number increased. The behavior shown in **Fig. 29** agrees with the present work results that shown in **Fig. 26** (the mean Nusselt number increases as Rayleigh number is increased for the same Reynolds number value) and in **Fig. 27** (the mean Nusselt number increases as Reynolds number is increased for the same Rayleigh number value).

6. CONCLUSIONS

The main conclusions of the present work are:

1- The temperature difference (ΔT_w) increases as the imposed heat flux is increased.
2- For low Reynolds number (Re_d=14.62) and with higher buoyance effect, the temperature difference (ΔT_w) exhibit a moderate fluctuation with the axial distance.
3- For high Reynolds numbers (Re_d=19.48 and 24.36) and with higher effect of the inertia force of the incoming cold-fluid, the temperature difference (ΔT_w) increased with the axial distance and reached a maximum value at Z=0.2m from the annulus entrance section and then it decreased downstream up to the annulus exit section.
4- At low heat fluxes [q_w = 3912 W/m^2 and 5511 W/m^2], the temperature difference (ΔT_w) decreased as the Reynolds number increased. On the other hand, for higher heat fluxes [q_w = 7382 W/m^2 to 11907 W/m^2] a gradual inversion can be seen in which the temperature difference (ΔT_w) decreased as the Reynolds number decreased due to the domination of the buoyancy force over the inertia force of the incoming cold-fluid.
5- The local heat transfer coefficient increased with the increased of the imposed heat flux and Reynolds number.
6- Mean Nusselt number is increased with the increased of Rayleigh number and Reynolds number.

REFERENCES

- Andrea, D., Simone, M., Claudio, Z., Luisa, R., 2012, *Experimental Measurements of Air Forced Convection through Copper Foams*, International Refrigeration and Air Conditioning Conference at Purdue, July 16-19, 2312.
- Boomsma, K., and Poulikakos, D., 2002, *The effects of compression and pore size variations on the liquid flow characteristics in metal foams*, ASME J. Fluids Eng. 124, pp. 263–272.
- D. A. Nield, A. Bejan, 2006, *Convection in porous media*, New York, Springer.
- Dirker. J., and Vyver. H. V. 2004, *Convection Heat Transfer in Concentric Annuli*. Experimental Heat Transfer, Volume 17, Issue 1, pp. 19 - 29.
- Hussein, M. A., Tahseen, A. T., and Jasim, H. A., 2009, *Convection Concentric Annulus Vertical Cylinders Filling Porous Media*, Journal of Kirkuk University-Scientific Studies, vol.4, No.2, pp. 55–71.
- K. Muralidhar, 1988, *Mixed convection flow in a saturated porous annulus*, International Journal of Heat Mass Transfer,Vol. 32, pp. 881–888.
- Pu, W. L., Cheng, P., Zhao, S. T., 1999, *An Experimental Study of Mixed Convection Heat Transfer in Vertical Packed Channels*, ALAA Journal of Thermo Physics and Heat Transfer, Vol. 13 (4), pp. 517 – 521.
- Renken, K. J., and Poulikakos, D., 1990, *Mixed convection experiments about a horizontal isothermal surface embedded in a water-saturated packed bed of spheres*, International Journal of Heat Mass Transfer,Vol. 33, pp. 1370–1373.
- Venugopal, G., Balaji, C., Venkateshan, S. P., 2010, *Experimental Study of Mixed Convection Heat Transfer in a Vertical Duct Filled with Metallic Porous Structures*, International Journal of Thermal Sciences, Vol. 49, pp. 340-348.

8. NOMENCLATURE

A = area, m^2.
β = expansion coefficient, K^{-1}.
d_p = mean diameter, m.
D_h = hydraulic diameter, m.
ε = porosity.
K = absolute pearmability, m^2.
k_{eff} = effective thermal conductivity, W/m^2. K.
Gr = Grashof number.

h = local heat transfer coefficient, W/m^2.K.
L = effective heating length, m.
Nu = Nusselt number.
Pr = Prandtl Number.
ρ = density, kg/m^3.
Ra = Rayleigh number.
q_w = heat flux, W/m^2.
Q = volumetric flow rate, L/min.
Re_d = Reynolds number based on the particle diameter.
T = temperature, K.
U_{in} = inlet velocity, m/s.
v = kinematic viscosity, m^2/s.
Vol_{solid} = volume of the metallic porous media, m^3.
Vol_{total} = total volume of the concentric annulus, m^3.

Subscript Meaning

b = bulk.
m = mean.
w = wall.

Table 1. Thermophysical properties of the water- stainless steel beads system.

Property	Symbol	Solid	Liquid
Density	ρ kg/m^3	7833	988.1
Thermal conductivity	k W/m K	15.1	0.644
Expansion coefficient	β, K^{-1}	---	0.451×10^{-3}
Dynamic viscosity	μ kg/m.s	---	0.547×10^{-3}
Prandtl Number	Pr	---	3.55

Table 2. Physical parameters for each size of the copper beads.

Mean diameter d_p (mm)	Porosity† ε	Permeability †† K (m^2)
6	0.4	3.556×10^{-6}

† Calculated experimentally with the use of Eq. (4).
†† Calculated from Eq. (2).

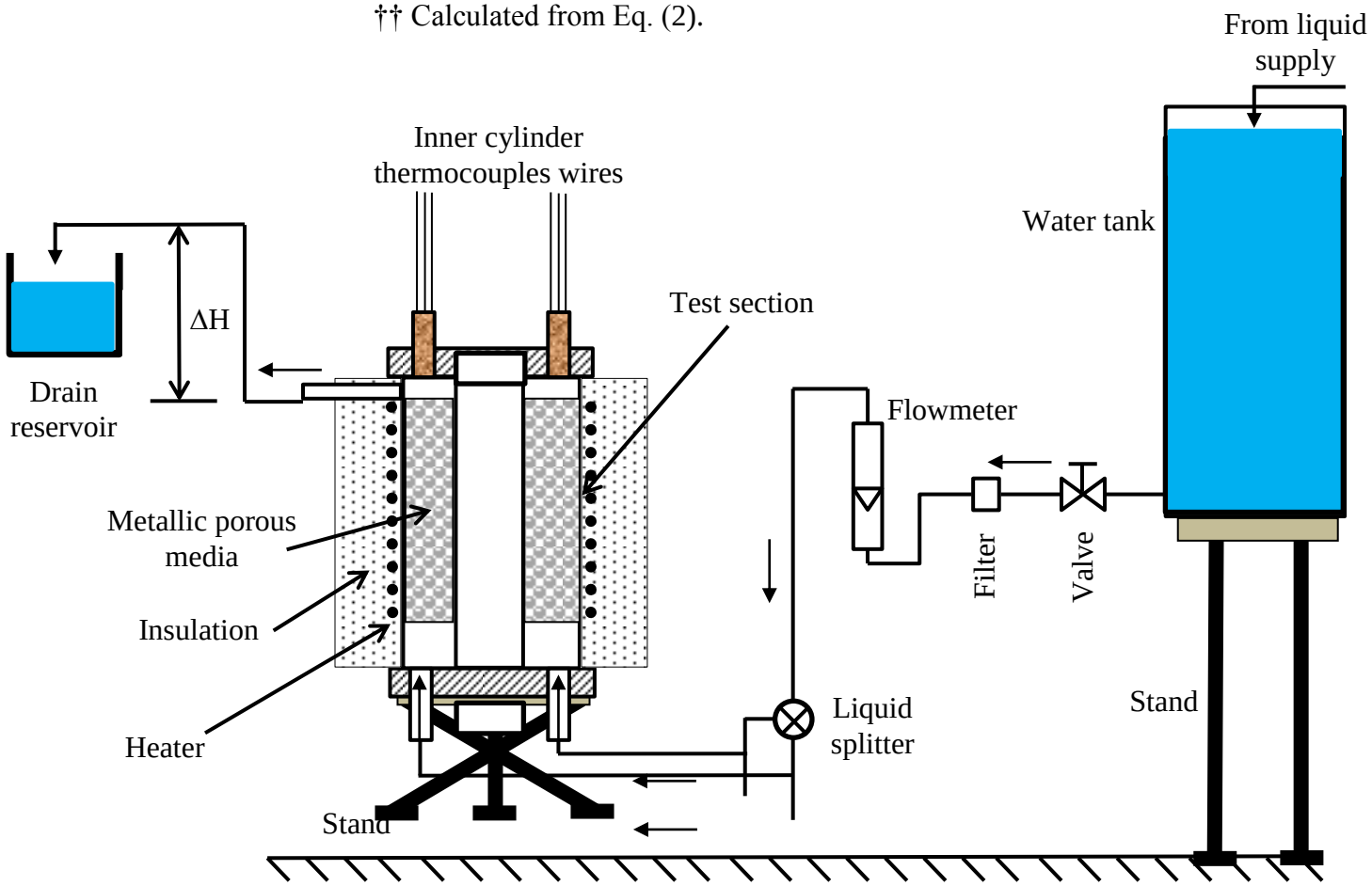

Figure 1. Schematic of the experimental apparatus.

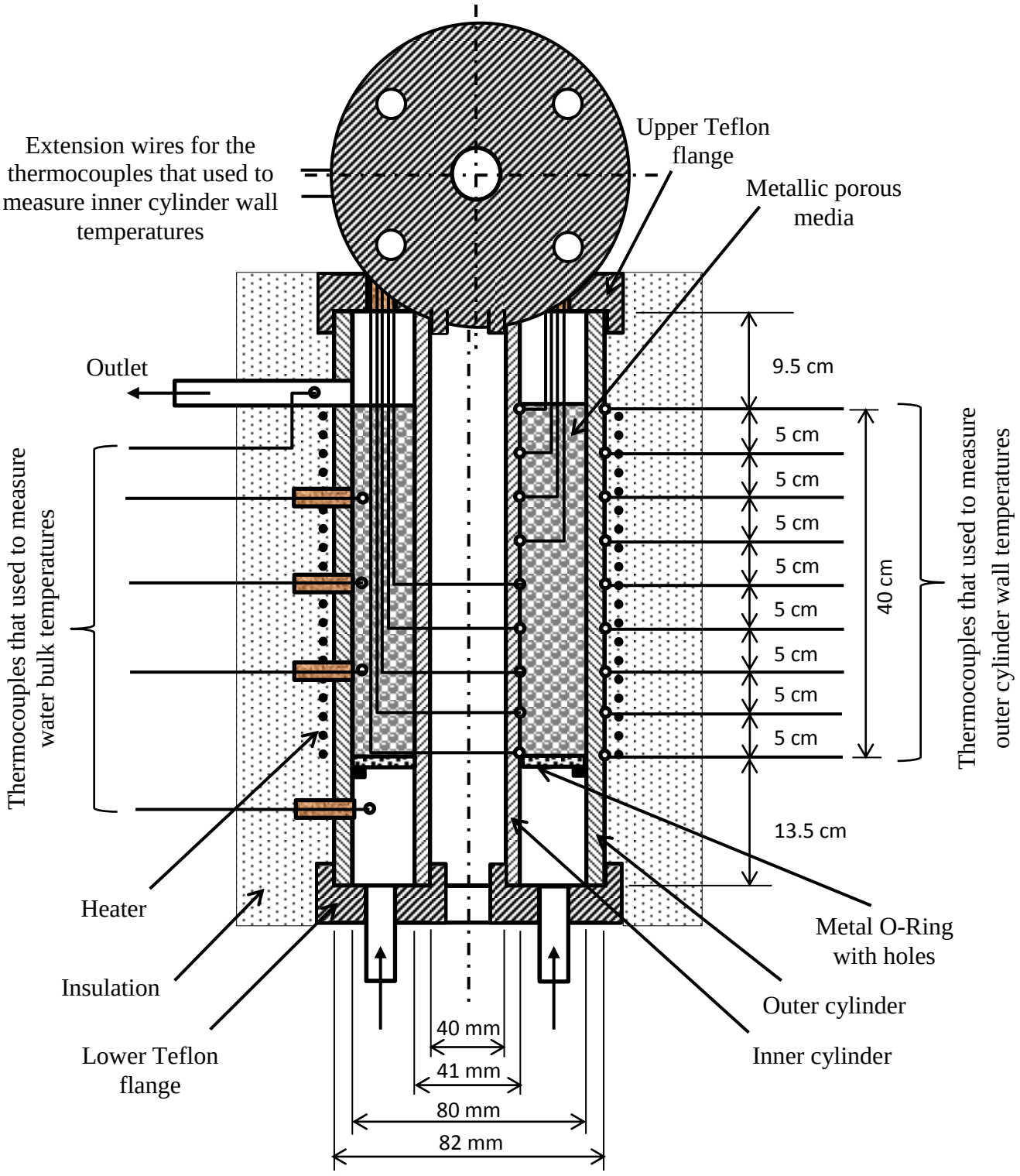

Figure 2. Arrangement and the locations of thermocouples.

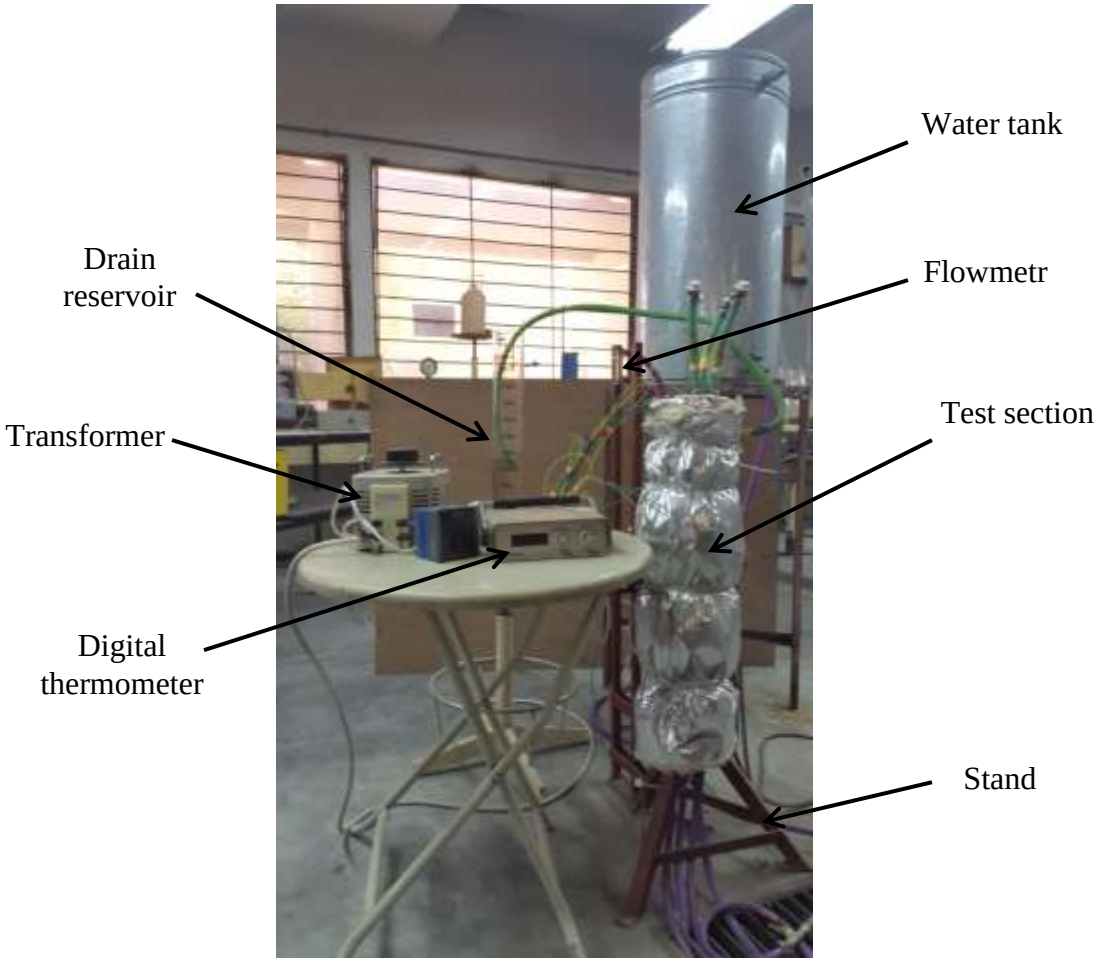

Figure 3. Photograph of the experimental apparatus.

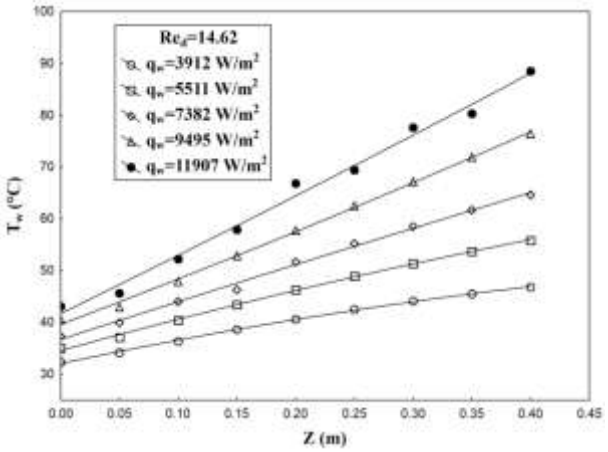

Figure 4. Variation of the outer annulus surface temperature with the axial distance for different heat fluxes and Re_d=14.62.

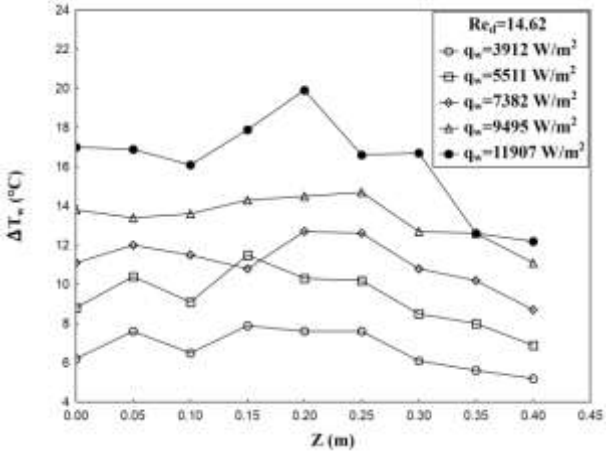

Figure 7. Temperature difference between inner and outer annulus surfaces with the axial distance for different heat fluxes and Re_d=14.62.

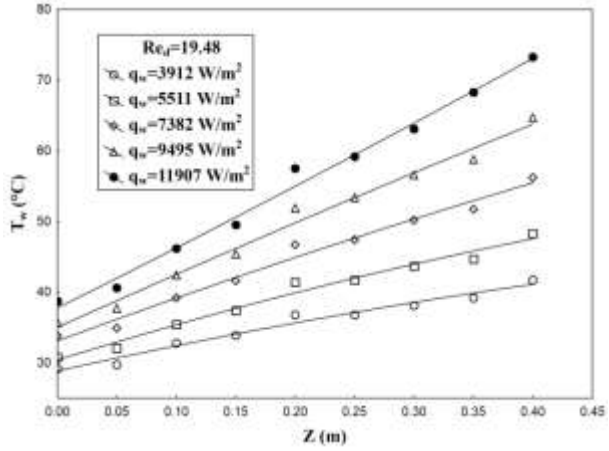

Figure 5. Variation of the outer annulus surface temperature with the axial distance for different heat fluxes and Re_d=19.48.

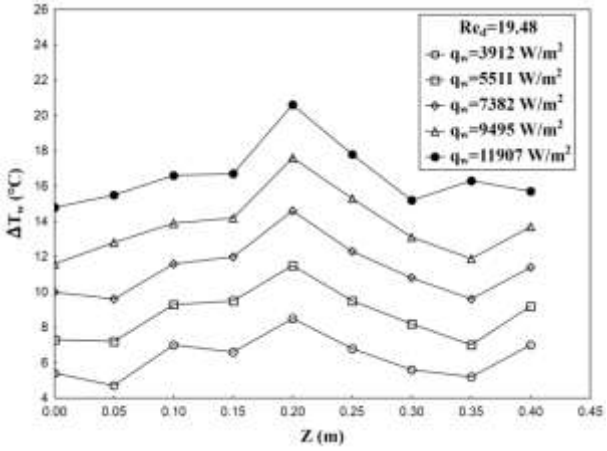

Figure 8. Temperature difference between inner and outer annulus surfaces with the axial distance for different heat fluxes and Re_d=19.48.

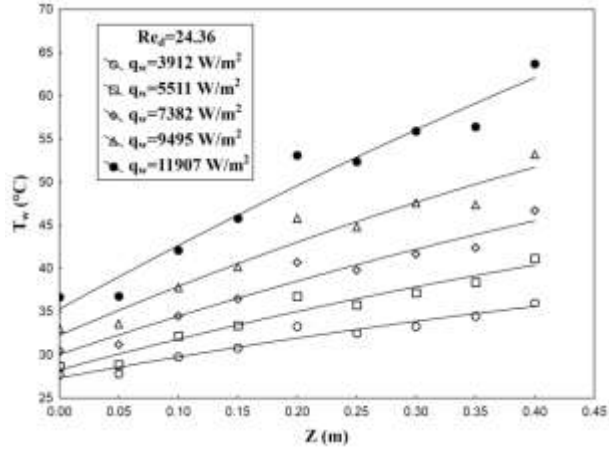

Figure 6. Variation of the outer annulus surface temperature with the axial distance for different heat fluxes and Re_d=24.36.

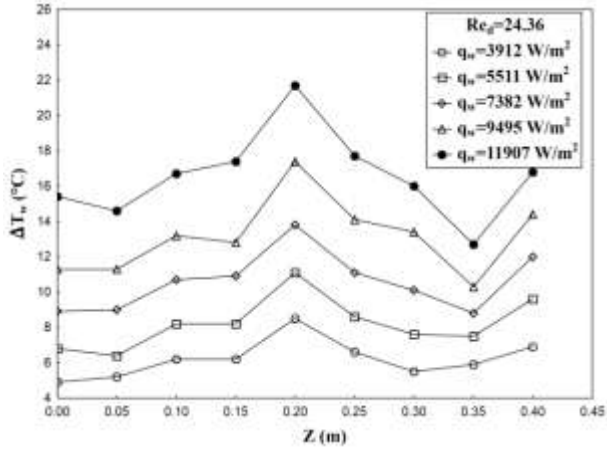

Figure 9. Temperature difference between inner and outer annulus surfaces with the axial distance for different heat fluxes and Re_d=24.36.

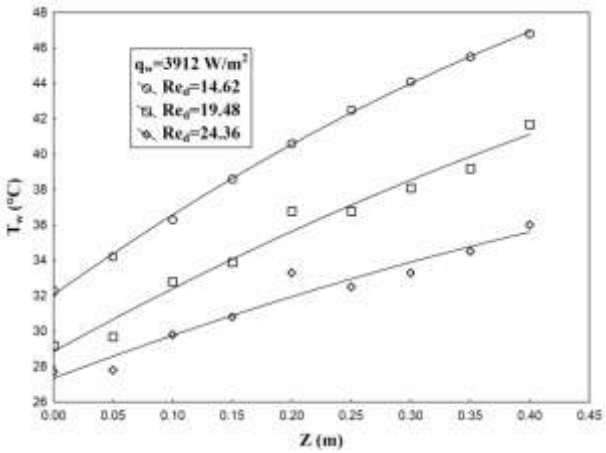

Figure 10. Variation of the outer annulus surface temperature with the axial distance for different Reynolds numbers and q_w=3912 W/m^2.

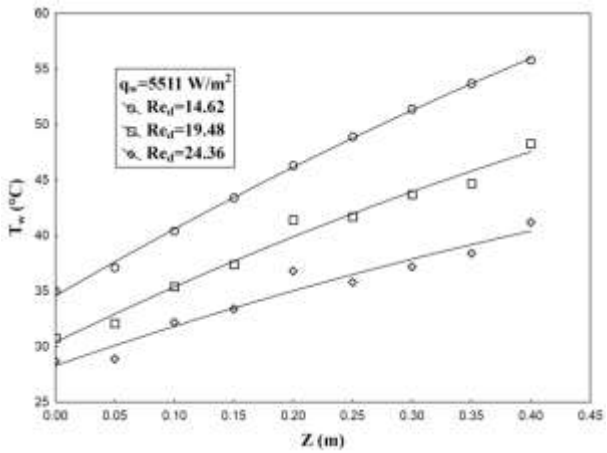

Figure 11. Variation of the outer annulus surface temperature with the axial distance for different Reynolds numbers and q_w=5511 W/m^2.

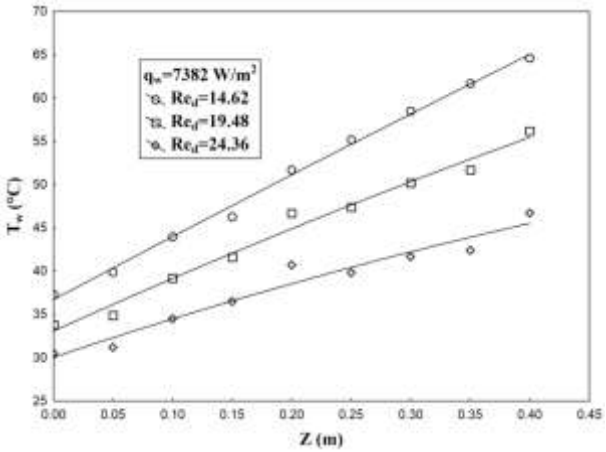

Figure 12. Variation of the outer annulus surface temperature with the axial distance for different Reynolds numbers and q_w=7382 W/m^2.

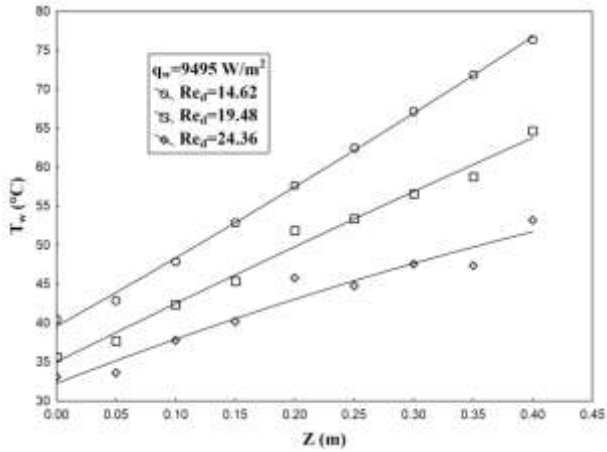

Figure 13. Variation of the outer annulus surface temperature with the axial distance for different Reynolds numbers and q_w=9495 W/m^2.

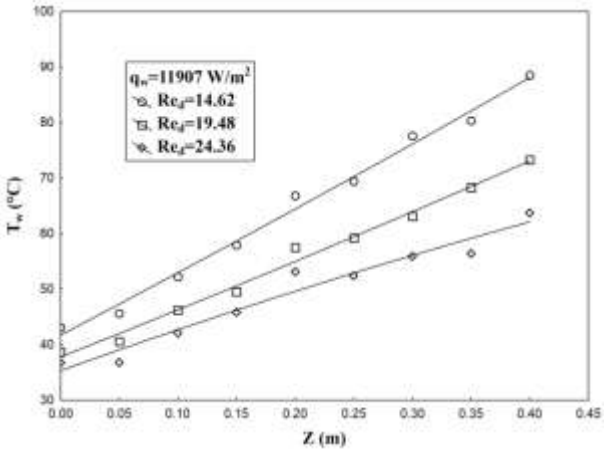

Figure 14. Variation of the outer annulus surface temperature with the axial distance for different Reynolds numbers and q_w=11907 W/m^2.

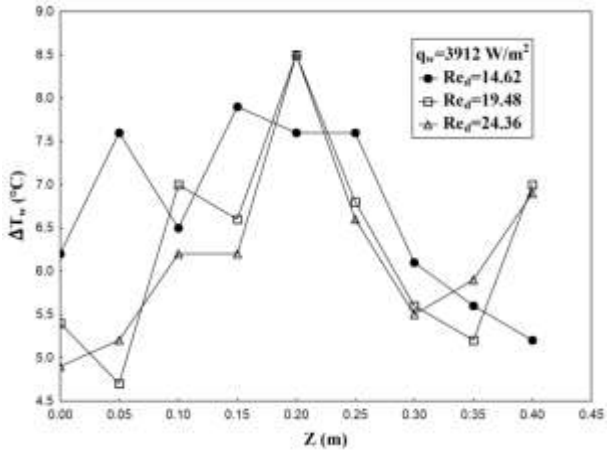

Figure 15. Temperature difference between inner and outer annulus surfaces with the axial distance for different Reynolds numbers and q_w=3912 W/m^2.

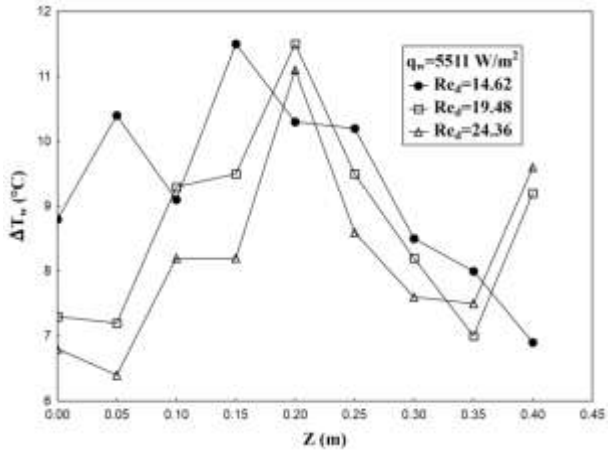

Figure 16. Temperature difference between inner and outer annulus surfaces with the axial distance for different Reynolds numbers and q_w=5511 W/m^2.

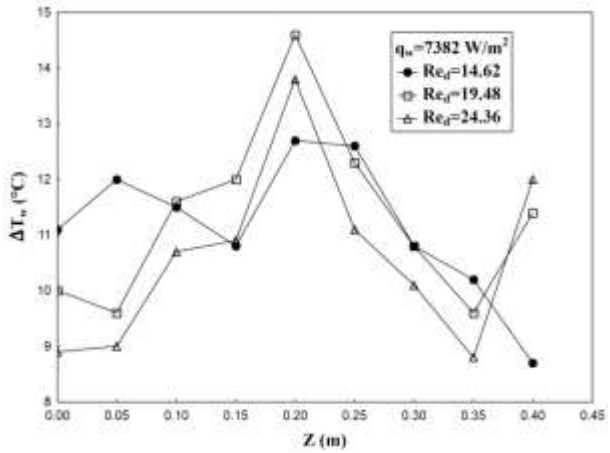

Figure 17. Temperature difference between inner and outer annulus surfaces with the axial distance for different Reynolds numbers and q_w=7382 W/m^2.

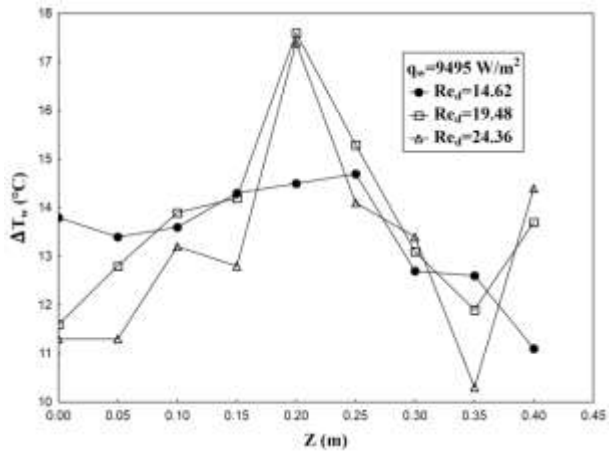

Figure 18. Temperature difference between inner and outer annulus surfaces with the axial distance for different Reynolds numbers and q_w=9495 W/m^2.

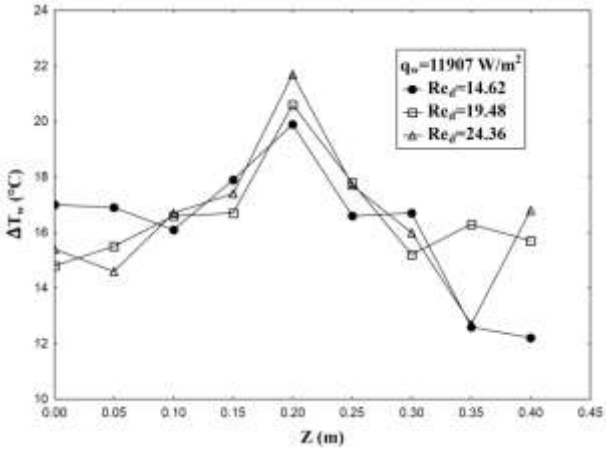

Figure 19. Temperature difference between inner and outer annulus surfaces with the axial distance for different Reynolds numbers and q_w=11907 W/m^2.

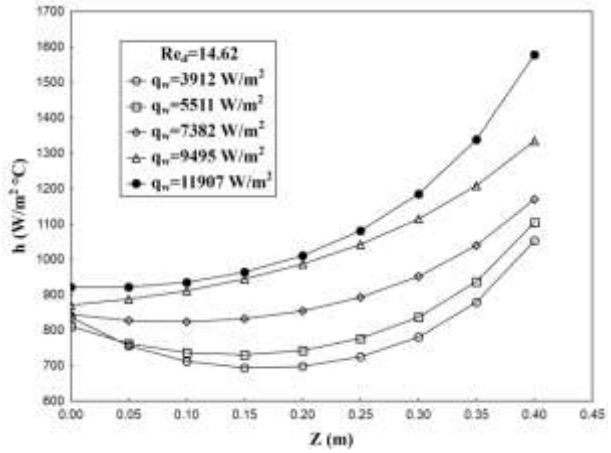

Figure 20. Local heat transfer coefficient with the axial distance for different heat fluxes and Re_d=14.62.

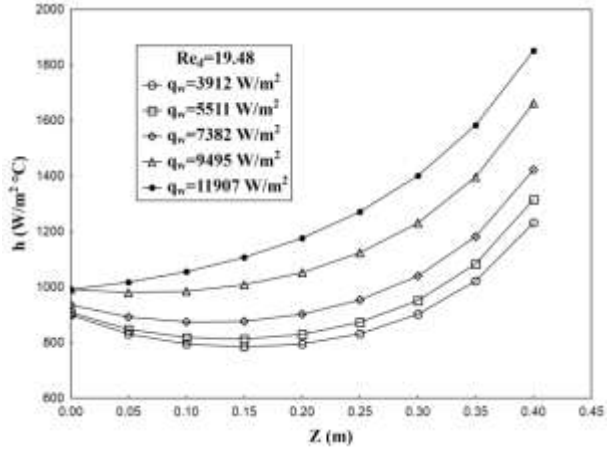

Figure 21. Local heat transfer coefficient with the axial distance for different heat fluxes and Re_d=19.48.

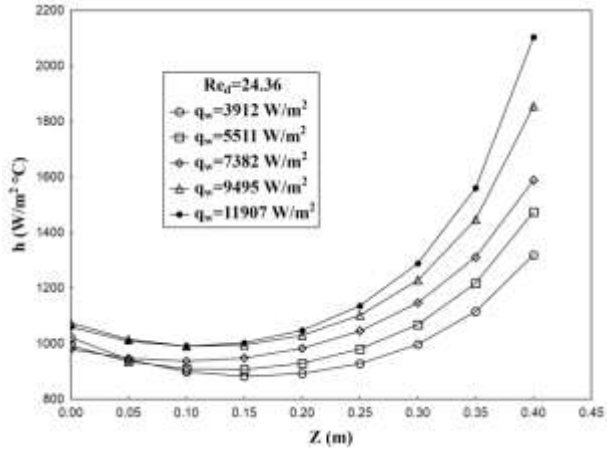

Figure 22. Local heat transfer coefficient with the axial distance for different heat fluxes and Re_d=24.36.

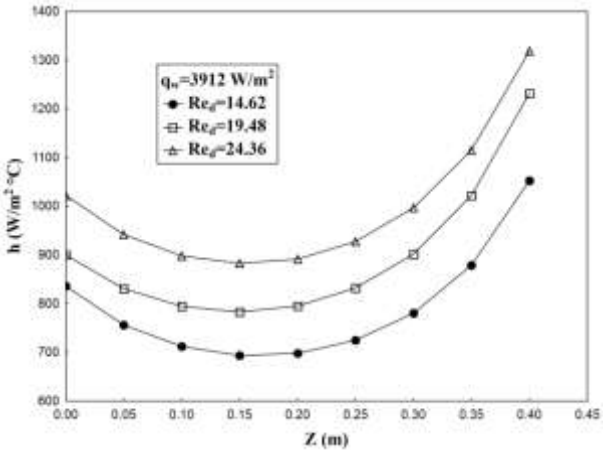

Figure 23. Local heat transfer coefficient with the axial distance for different Reynolds numbers and q_w=3912 W/m^2.

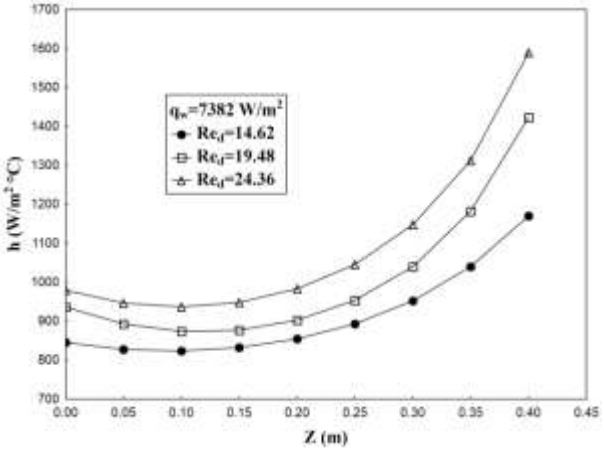

Figure 24. Local heat transfer coefficient with the axial distance for different Reynolds numbers and q_w=7382 W/m^2.

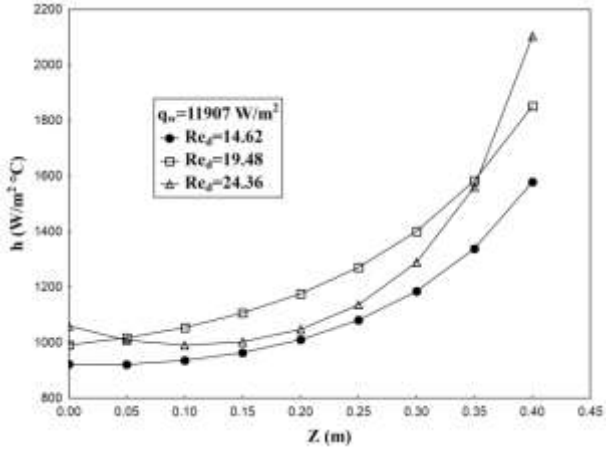

Figure 25. Local heat transfer coefficient with the axial distance for different Reynolds numbers and q_w=11907 W/m^2.

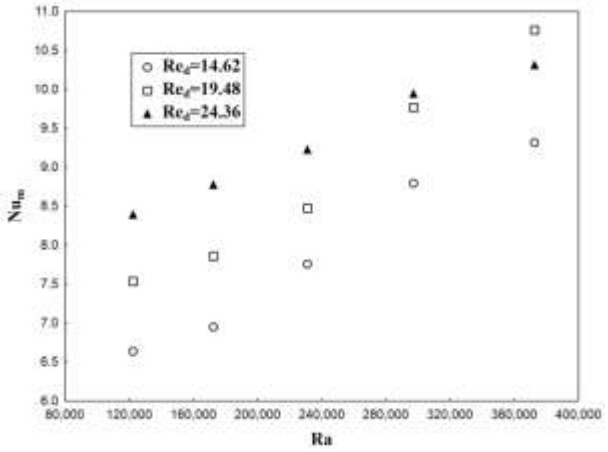

Figure 26. Mean Nusselt number versus Rayleigh number for different Reynolds numbers.

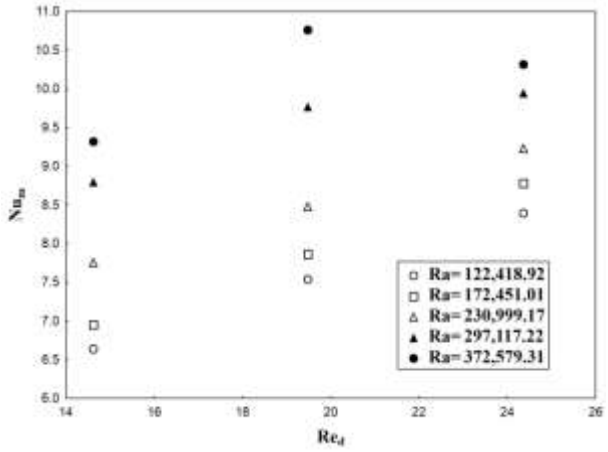

Figure 27. Mean Nusselt number versus Reynolds number for different Rayleigh numbers.

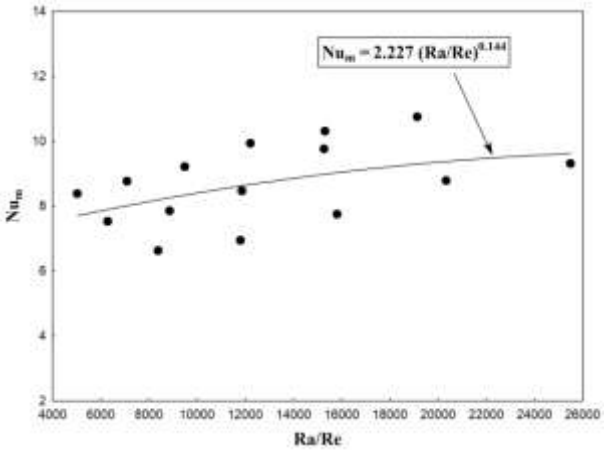

Figure 28. Mean Nusselt number versus Ra/Re.

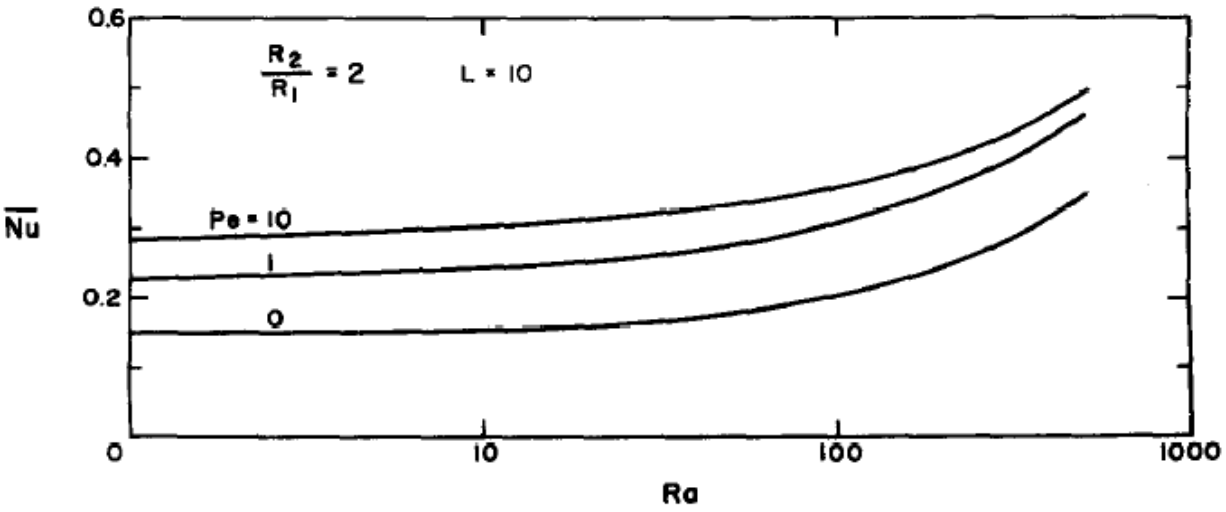

Figure 29. Average Nusselt number of a vertical annulus as a function of Rayleigh number (**K. Muralidhar, 1988**).